JOURNAL OF THERMOPHYSICS AND HEAT TRANSFER
Vol. 21, No. 3, July–September 2007

Analyses of Numerical Errors in the Kinetic Modeling of Microthruster Devices

E. Titov* and D. Levin†
Pennsylvania State University, University Park, Pennsylvania 16802
and
Sergey V. Rogazinsky‡
Institute of Computational Mathematics and Mathematical Geophysics, SB RAS, 630090, Novosibirsk, Russia

DOI: 10.2514/1.28737

A comprehensive numerical analysis of a three-dimensional microelectromechanical system-based micropropulsion system has been performed using the direct simulation Monte Carlo method. The transitional flow regime in the viscous nozzle flow prevents the use of Navier–Stokes based approaches, but the flow is still computationally difficult for the direct simulation Monte Carlo method. The numerical aspects of the direct simulation Monte Carlo approach are sufficiently challenging such that the traditional manner of establishing numerical convergence by observing the lack of change in the solution for increased numbers of computational particles and cells, even for a computation of 130×10^6 particles, fails. Therefore to obtain confidence in the presented results, a better understanding of the nature of the computational errors is necessary. The statistical and deterministic error analyses provided in this article allow us to support the validity of the presented results for low stagnation pressure microelectromechanical system micronozzle flows as well as to suggest a procedure for evaluating numerical errors for other computationally difficult, viscous microdevice flows being solved by the direct simulation Monte Carlo method.

Nomenclature

A_{DSMC}	=	computed solution (the value of a macroparameter in a cell)
A_0	=	extrapolated solution (the true value of a macroparameter in a cell)
A_1, A_2, A_3	=	errors (due to the time step, cell sizes, and number of particles, respectively)
$Err(X)$	=	error of the computed property
k_B	=	Boltzmann's constant
L	=	number of series
M_s	=	number of time steps in the series
m	=	mass per molecule
N	=	total number of simulated particles
N_k	=	number of particles in the particular cell of interest during the kth time step
N_s	=	sample size
N_t	=	number of time steps
T	=	temperature
v_x, v_y, v_z	=	velocity components of the particles
X	=	computed or true property
Δt	=	time step
ΔV	=	cell volume
σ_X^2	=	variance of the computed property

Subscript

i	=	index of the molecule

Received 7 November 2006; revision received 30 January 2007; accepted for publication 30 January 2007.

*Graduate Student, Department of Aerospace Engineering. AIAA Student Member.
†Associate Professor, Department of Aerospace Engineering. AIAA Associate Fellow.
‡Senior Researcher, Laboratory of Monte Carlo Methods.

I. Introduction

NEW microelectromechanical system (MEMS)-based micropropulsion systems capable of delivering precise impulses for small spacecraft maneuvers have been recently developed [1]. The advantages of MEMS-based micropropulsion devices include weight reduction through the use of lightweight materials, the ability to provide versatile thrust levels, and the potential of using such devices to permit microsatellite constellation clustering [2]. Micronozzle devices will operate over a range of pressures from approximately 0.1 to 5 atm, with the actual stagnation pressure depending on the specific mission requirements. A wide range of the flow regimes exists in the subsonic and supersonic regions of the MEMS device [3]. Although Navier–Stokes (NS) computational fluid dynamics (CFD) techniques are able to solve the higher pressure stagnation cases, they fail to capture the flow physics for the low pressure stagnation cases and therefore the direct simulation Monte Carlo (DSMC) method, based on the kinetic theory, must be applied. At the same time, it is the coupling of the flow viscosity and the rarefaction that pose the main computational challenge for the DSMC method which becomes computationally too expensive in the most dense portions of the flow. For the above range of stagnation pressure conditions, the physics and performance of the micronozzle are dominated by the properties of the viscous boundary layer [4,5].

Experimental data on micronozzle systems have been obtained by several investigators [6–8]; however, detailed flow and nozzle exit quantities such as mass flow rate and thrust are not available for all stagnation conditions. Moreover, the experimental investigation of fluid flow and performance of microthrusters is hindered by large measurement uncertainties at this small scale. Hence, accurate modeling and simulation are crucial for assessing performance and improving system designs. However, numerical studies of the semirarefied flows in MEMS devises are very expensive and are often limited by the available computational power. The computational nature of the problem restricts the use of traditional DSMC numerical solution convergence tests and proof of convergence may be difficult. Our goal is to develop a better understanding of the nature of the numerical errors, grouping them into categories of statistical and deterministic. With this improved understanding, the solutions obtained from the DSMC modeling of

low pressure MEMS devices may be used to predict nozzle performance with greater confidence.

In earlier work, MEMS-based propulsion systems were modeled in [3–5]. It was shown in these papers that the flowfields were sensitive to the fidelity of the modeling especially with respect to approximating three-dimensional flows as two dimensional and the need to couple the flow simulation with the modeling of the flow-wall heat exchange. Both of these factors were found to affect the predicted nozzle thrust and mass flow rates. In this paper we are focused on a different aspect of the problem. Our goal here is to test the numerical limits of the DSMC method, solving the flow in a three-dimensional micronozzle device with high accuracy to analyze the sources of computational errors. We show in this paper that the influence of the numerical parameters of the DSMC method can change computed flow parameters quantitatively and has an impact on the predicted device performance. By the analyses of results obtained from several computations with different numerical scheme parameters, we show that it is possible to understand if the results obtained are linearly dependent on the scheme parameters. Such an analysis allows us to adjust these numerical parameters in a quantitative way and to extrapolate the final solution to the problem using the available solutions in cases where the final result may not be computed with a sufficiently large number of computational particles and cells directly.

We study a micronozzle device, developed recently by researchers at the NASA John H. Glen Research Center [1]. The device is a micronozzle with a characteristic size on the order of hundreds of microns and a stagnation pressure level of 0.1 atm. The device has a 3-D internal shape with a depth (the third dimension) that is relatively small. For the flow regime and the surface-volume ratio of the device, it can be expected that there will be significant boundary layer growth along the nozzle walls, preventing the use of a simplified 2-D model of the computational domain [3]. The small nozzle depth also poses additional challenges for the NS technique with the velocity, no-slip boundary condition giving unphysical results. Although it should be noted that a slip–jump boundary condition correction to the Navier–Stokes equations, not tested in this work, might also provide good solutions for the 0.1 atm stagnation pressure condition. In this study we apply the DSMC method to solve the flowfield and obtain the device parameters, investigate the limits of applicability of the DSMC method to MEMS microthruster related flow problems, and provide an error analysis for the limiting cases to understand the reliability of the obtained solutions. The remainder of the paper is organized as follows. In Sec. II we present the theoretical background related to the statistical and deterministic error analysis performed in this work. We discuss the device parameters as well as the specifics of implementation of the DSMC method to quantify the numerical errors, while simultaneously solving the device flow in Sec. III. Errors related to the selection of specific numerical scheme parameters are known to exist, but are rarely, if ever, quantified for a realistic three-dimensional flow due to large computational time and storage requirements. In Sec. IV we present the numerical parameters of the scheme, discuss the results of the obtained solutions, and provide the error analysis. Finally we provide conclusions in Sec. V.

II. DSMC Method and Analyses of Errors

The DSMC method of Bird [9] is a statistical approach used to solve the Boltzmann equation which describes the discrete nature of rarefied gases. Most DSMC algorithms require time and space discretization. The steps in such a discretization must be on the order of the time necessary for a molecule to collide and the mean free path of the molecules to ensure that the predicted flow parameters correspond to a solution of the Boltzmann equation. The values of the mean free path depend on the flow pattern and therefore it is a good practice to choose the collisional cell size locally. However, in doing so, one must make sure that the number of computational particles in a collision cell is sufficient to obtain a physically reasonable result. The traditional method of establishing convergence is to increase the number of particles and cells in the computational domain until the flowfield does not change. For computationally intensive systems, however, this brute force approach will not work. Therefore, one needs to understand, quantify, and predict the main types of errors: 1) a statistical error which corresponds to the stochastic nature of the method, and 2) a deterministic error which depends on the selection of numerical parameters such as Δt, ΔV, and N. One has to be able to separately analyze those errors to understand their influence on the flow results [10,11].

First, let us consider errors due to the stochastic nature of the DSMC method. The steady state flow macroparameters are obtained by averaging the particle properties, such as number density and velocity, over N_t. Therefore, the source of the statistical errors is due to the process of taking a sample average in a finite volume. The errors have an asymptotic behavior and vanish when the sample size goes to infinity. Thus, these errors are inversely proportional to square root of the sample size, and therefore they may be decreased by increasing of the sample size, that is, the number of particles in a computational domain or number of time steps used in the sample. Usually we can assume that the variance of X is independent of the sample size, and therefore this parameter has a statistical error,

$$|X_{\text{computed}} - X_{\text{true}}| \leq 3 \cdot \sqrt{\frac{\sigma_X^2}{N_s}} \tag{1}$$

where $\sigma_X^2 = E\{X^2\} - E^2\{X\}$ is the variance (dispersion) of X, $E\{X\}$ denotes the mean (expectation) of X. Equation (1) is the so-called three-sigma rule [12]. All definitions and notations from statistics can be found in [12–14]. Thus, by estimation of the variance σ_X^2, one can make an error prediction for a given sample size Err,

$$Err(X) = \frac{|X_{\text{computed}} - X_{\text{true}}|}{\bar{X}_{\text{computed}}} \tag{2}$$

The numerical errors corresponding to the stochastic nature of the DSMC method can be characterized by the variance of numerical results which may be obtained concurrent with the ongoing calculation. The micronozzle translational temperature fields were found to be more sensitive to the selection of DSMC numerical parameters than pressure or velocities, as may be expected because temperature is proportional to the second moment of the distribution function. Hence, we use this macroparameter to illustrate both the statistical and deterministic numerical errors. The empirical estimation of the temperature variance estimated over M_s time steps in a given cell is

$$T_{M_s} = \frac{m}{3k_B} \frac{\sum_{k=1}^{M_s} \sum_{i=1}^{N_k} \left(v_{x_i}^2 + v_{y_i}^2 + v_{z_i}^2 \right)}{\sum_{k=1}^{M_s} N_k} \tag{3}$$

where v_{x_i}, v_{y_i}, and v_{z_i} are the velocity components of the particles, the inner summation (i) is over particles during the kth time step, and the outer summation is over time steps. One needs to repeat the procedure given by Eq. (3) for calculating T_{M_s} L times, where L is the same as N_s in Eq. (1). With these definitions, the empirical variance of the temperature series is calculated as $\sigma_{T_{M_s}}^2 = E\{T_{M_s}^2\} - E^2\{T_{M_s}\}$, and represents the variance of temperature computed over M_s time steps. Thus, the temperature error per time step in a cell normalized by $\overline{T_{M_s}} = E\{T_{M_s}\}$ is

$$Err(T_{M_s}) = 3 \cdot \frac{\sqrt{\sigma_{T_{M_s}}^2}}{\sqrt{L} \cdot \overline{T_{M_s}}} \tag{4}$$

Secondly, we consider errors that occur because the numerical parameters cannot be taken as infinitesimally small. These errors are not statistical in nature, and therefore cannot be reduced by use of a large sample size. In fact, this type of error may have a greater impact on the results than the statistical error, especially when the sample size N_s is large enough such that statistical errors become small compared to deterministic errors. Assuming that the parameters Δt, ΔV, and N^{-1} are small, the estimated flow macroparameter A in each cell can be approximated as a linear function (neglecting cross terms

and higher order terms) of these parameters as

$$A_{\mathrm{DSMC}}(\Delta t, \Delta V, N^{-1}) = A_0 + A_1 \cdot \Delta t + A_2 \cdot |\Delta V| + A_3 \cdot N^{-1} \tag{5}$$

where, in general, coefficients A_0, A_1, A_2, A_3 are functions of the cell location in the computational grid. In particular, A_0 stands for the exact solution, A_{DSMC} is the DSMC computed macroparameter, and the rest of the terms in Eq. (5) represent the deviation of A from the exact solution. By performing DSMC calculations for different numerical parameters, one can study the dependence of the flow solution on these parameters as well as estimate the true solution, A_0. Essentially, one can obtain a number of sequential solutions to the problem with increasingly smaller cell sizes, time step, and larger numbers of particle per cell. Even if the most expensive solution that may be performed is not the final, converged solution, the macroparameters obtained from sequential DSMC solutions are used in the left-hand side (LHS) of Eq. (5), along with the specific numerical values of Δt, ΔV, and N, to approximate the exact solution, A_0. However, the selection of numerical parameters must be reasonably good to ensure that the linear approximation used in Eq. (5) holds. For example, the time step Δt and the cell size ΔV should be chosen sufficiently small compared to the characteristic time and length scale of the flow under consideration. The number of particles in a cell N should be sufficiently large to prevent correlations between particles and to satisfy the requirements of DSMC schemes, such as the majorant frequency scheme (MFS) of Ivanov and Rogasinsky [15] or the no-time-counter (NTC) scheme of Bird [9].

In CFD methods the size of the finite-difference cells causes discretization errors between the numerical solution to the differential equations and their exact solutions [16]. Again, due to computational limitations, it is often possible that a mesh independent solution is not achievable and an estimate of the possible residual error in the solutions is necessary. The Richardson extrapolation technique is often used to approximate the final solution by the available preliminary results [17]. The form and application of Eq. (5) to the DSMC method is similar to that of the Richardson extrapolation procedure except that the DSMC procedure employs a discretization of time, cell size, and a finite number of computational particles N to represent the kinetic structure of the gas. Note that although CFD methods also use a finite time step, the criteria for its selection is different from that of DSMC.

III. Nozzle Geometry and Flow Conditions

The geometry of the micronozzle considered in this work is the same as that developed by NASA Glenn researchers [1]. The configuration of the nozzle can be seen in Fig. 1 where a schematic of the 3-D computational domain calculations is presented. The internal dimensions of the nozzle and the flow conditions studied in this work

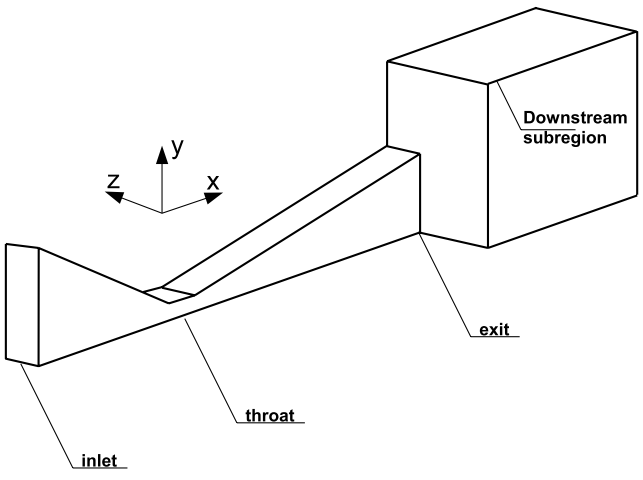

Fig. 1 Computational domain for the DSMC.

Table 1 Flow and nozzle conditions[a,b]

Length[a]:	2.44
Inlet height:	3.0
Throat height:	0.3
Exit height:	1.5
Thickness:	1.2
Stagnation pressure:	0.1 atm
Stagnation temperature:	2000 K
Gas	N_2

[a]The nozzle dimensions are given in mm.
[b]The background pressure is approximately zero.

are presented in Table 1. Note that the Knudsen number, defined here as the ratio of the mean free path to inlet thickness, is 0.01. In the prototype micronozzle device shown here, the high-temperature flow inside the microthruster would be generated by a laser-ignited solid monopropellant decomposition. Molecular nitrogen would be the major product of such a decomposition and hence is considered as the working gas in the current studies. The wall temperature is fixed at 300 K and diffuse reflection of the molecules at the nozzle walls (full accommodation) was assumed.

The flow in the presented nozzle is sufficiently viscous, and portions of the flow are in the transitional regime. Therefore a kinetic technique must be employed to accurately predict the device parameters in this case. For this condition, the micronozzle flowfields are calculated by a 3-D, DSMC approach. The SMILE [18] software which implements the majorant frequency scheme in DSMC [19] is used in these studies. The computational time step has been chosen to be the smallest possible for the available machine and was always smaller than required by the DSMC criteria so that its influence on the results can be safely excluded.

IV. DSMC Results and Error Estimations

The first DSMC calculation has been performed with a reasonable yet relatively small amount of 1.3×10^6 particles and 670,000 cells. It should be noted that SMILE software adopts the computational grid to the flow gradients while keeping, at the same time, the average number of particles at about 4 to 5 in a computational cell. Therefore, further grid adaptation is usually enabled by adding more particles to the computational domain. This simple strategy must be employed until the calculated flow parameters, for example, the translational temperature, becomes insensitive to any further increase in the number of computational particles. Four computational runs with a gradual increase in the number of particles were performed. Table 2 summarizes the computational number of particles and cells for the four DSMC calculations presented in the subsequent figures. The first four cases used approximately 20,000 and 75,000 time steps before sampling, respectively. Note that the final increase in the number of particles is only a factor of 2 because the limits of the computational resources on the computer cluster were reached. It should be noted that the number of particles per computational cell was always kept sufficiently high in all of the four computational cases. Figure 2 shows the number of particles per cell throughout the flowfield at steady state for the most computationally expensive case, DSMC(4). The DSMC method also requires that the local (cell) Knudsen number be on the order of unity, or equivalently, that the local mean free path is approximate to the collision cell size. Figure 3

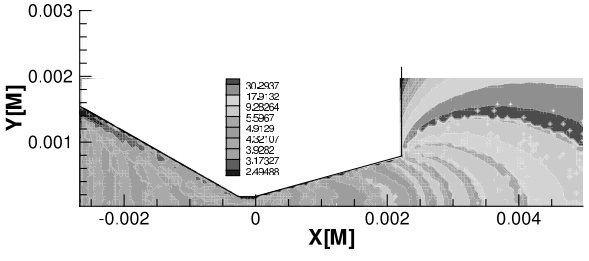

Fig. 2 Number of particles per cell, DSMC(4).

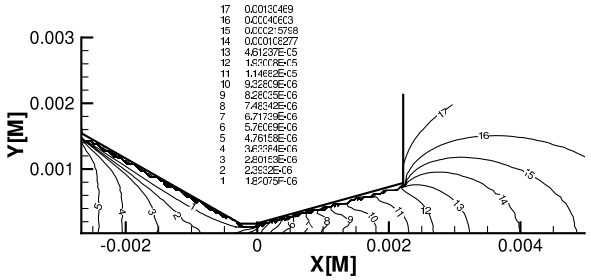

Fig. 3 Local mean free path, case DSMC(4).

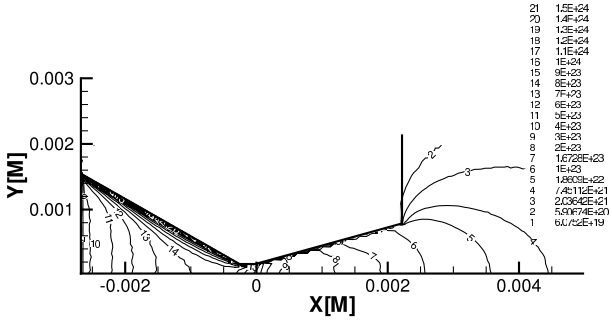

Fig. 4 Number density contours ($1 = 5.0e + 23$), case DSMC(4).

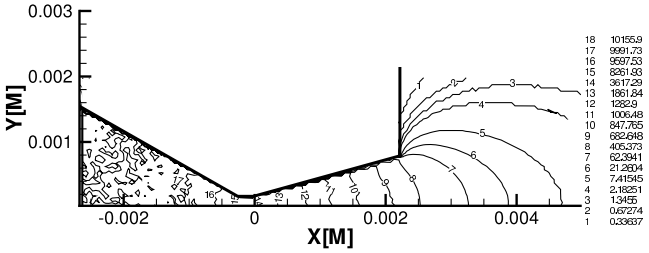

Fig. 5 Pressure contours, case DSMC(4).

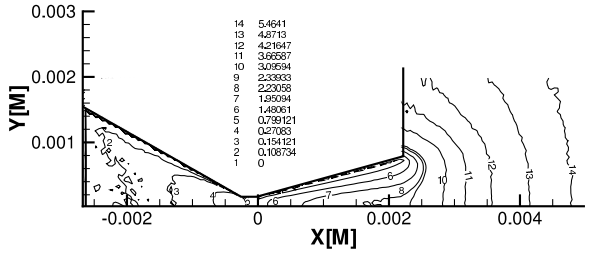

Fig. 6 Mach number contours, case DSMC(4).

shows the large variation in the local mean free path, again for DSMC case (4). Of all of the four cases, only for this computationally extensive case is the correspondence of the local mean free path to the collision cell size achieved.

The major flow parameters, density, pressure, Mach number, translational temperature, and x and y velocity components obtained from the solution of case DSMC(4) are presented in Figs. 4–9, respectively. (SI units are assumed throughout the paper.) The spatial dependence of the macroparameters presented in the figures is typical of the physics of micronozzle flows. All of the presented quantities (except for the pressure) show the development of a significantly thick boundary layer in both the sub- and supersonic portions of the nozzle. The pressure levels are approximately equal along nozzle cross sections, which again is in agreement with the physics of micronozzle flows. The Mach number reaches a value of 1 at the nozzle throat and then the flow becomes supersonic and accelerates further in the diverging portion of the nozzle, which confirms that the specific computational parameters are adequate to

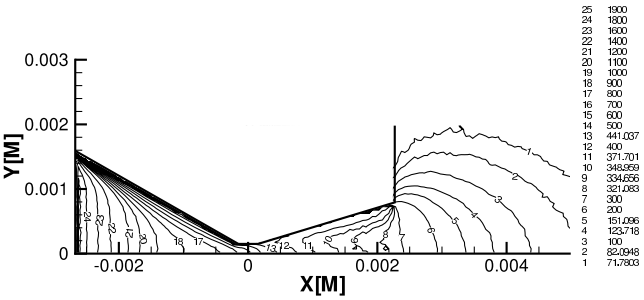

Fig. 7 Temperature contours, case DSMC(4).

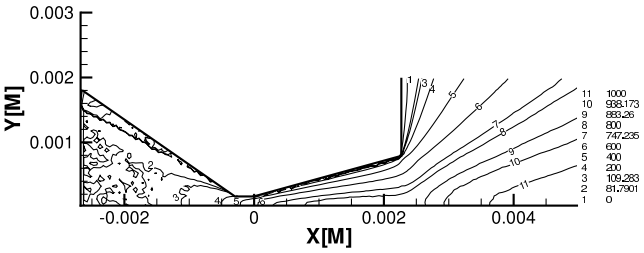

Fig. 8 X-velocity contours, DSMC(4).

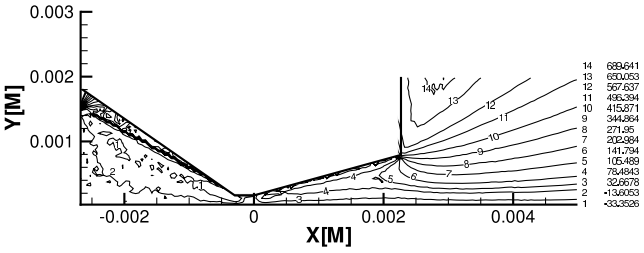

Fig. 9 Y-velocity contours, case DSMC(4).

model the physics of this highly viscous flow. As may be seen in Figs. 8 and 9, the flow accelerates farther due to its expansion into a vacuum, but this portion of the flow is not of interest in this study. Correspondingly, the gas pressures and temperatures drop, as Figs. 5 and 7 show, as the flow accelerates from the throat to the nozzle exit.

Let us now compare the macroparameters obtained with the different numerical parameters given in Table 2. Figure 10 presents the flow density contours obtained in the above-described first and fourth runs ($\sim 1.3 \times 10^6$ particles, $\sim 670,000$ cells, and 1.3×10^8 particles 5.23×10^7 cells, respectively). Even though the general shape of the number density contours is the same for both the runs, the boundary layer contours in the subsonic portion of the nozzle are different. The discrepancy between the simulation runs is more evident in the temperature and flow velocity profiles. Figure 11 presents translational temperature profiles perpendicular to the nozzle axis in the middle of its supersonic part ($x = 1.22$ mm) and Fig. 12 presents x-velocity profiles across the nozzle exit. Figure 13 shows the corresponding translational temperature profiles along the nozzle centerline, for all of the DSMC cases. The figures reveal physically correct flow features for all four cases for transitional, viscous micronozzle flow [4] caused primarily by the large surface to

Table 2 DSMC scheme parameters

Case	No. of particles[a]	No. of cells	Ratio[b]	Thrust, N
DSMC(1)	1.3×10^6	6.7×10^5	6.0×10^8	0.0014
DSMC(2)	1.2×10^7	5.6×10^6	6.0×10^7	0.0016
DSMC(3)	6.5×10^7	2.7×10^7	1.0×10^7	0.0017
DSMC(4)	1.3×10^8	5.23×10^7	5.0×10^6	0.0017

[a]Approximate number of computational particles at steady state.
[b]F_{num} = ratio of true particles to computational particles.

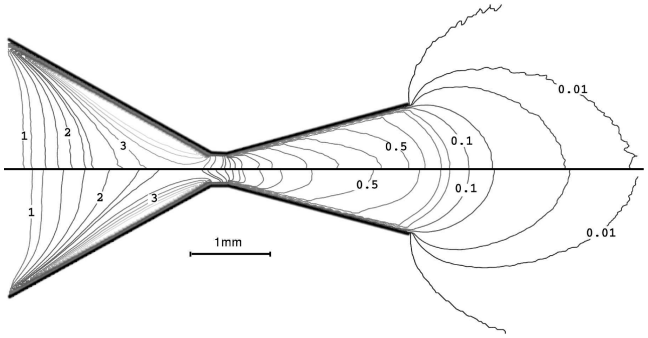

Fig. 10 Number density contours (1 = 5.0e + 23) top: case DSMC(1); bottom: case DSMC(4).

volume ratio found in MEMS devices. The effect of slip at the nozzle wall is visible in Figs. 11–13 showing that the presence of the thick boundary layer impedes the gas expansion through the nozzle. However, because the flow solution continues to change for the DSMC(1)–DSMC(4) cases, an error analysis is essential.

To obtain an estimation of the statistical errors, Eq. (3), we recorded the values of the macroparameters obtained during the DSMC(2) calculation. As soon as the case reached steady state (typically after approximately 20,000 time steps), we started to collect a series of independent massive sets of data ($L = 25$). For each group of $N_s = 1000$ time steps, we outputted the collected data set, reinitialized the arrays collecting particle information (such as the number of particles and velocities), and continued the calculation to obtain the next 1000-time step data set. In this manner we obtained 25 data sets and substituted the values of the temperature obtained in each computational cell from each of the 25 series into Eq. (3).

Figures 14 and 15 present contours of the relative error $Err(T_{M_s})$ and its dependence along the nozzle centerline, respectively. As can be seen in the figures, the statistical error remains small within the nozzle and increases immediately after the nozzle exit plane due to the rapid expansion of the flow and therefore a smaller sample size in this region of the computational domain. A small statistical error is obtained even for the DSMC(2) case, which has only about 12×10^6 particles.

Because the statistical error has been shown to be small, we now consider the role of deterministic errors. In the present study we were able to choose a time step $\Delta t = 2 \times 10^{-9}$ s, a value sufficiently small to eliminate the contribution of this parameter to the deterministic error for all of the simulations. Hence the coefficient A_1 may be set to zero in our analysis, leaving only the effect of the finite cell size and the number of particles on the solution A_2 and A_3, respectively. The values of ΔV and N^{-1} are obtained from the DSMC numerical

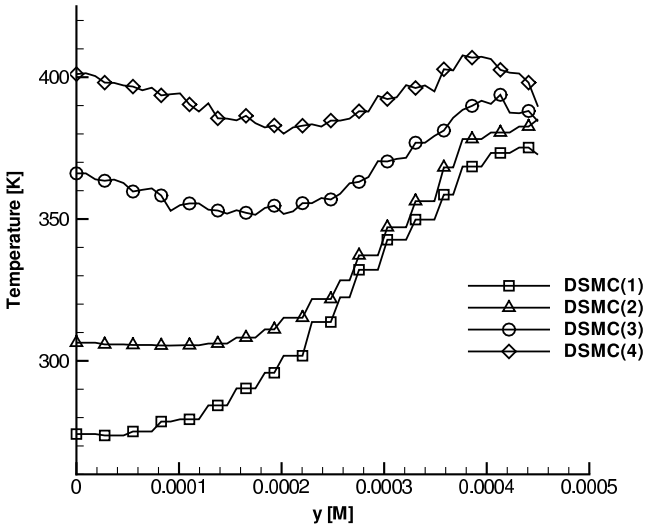

Fig. 11 DSMC, translational temperature across the nozzle in the middle of the supersonic part. The nozzle axis is located at $y = 0$.

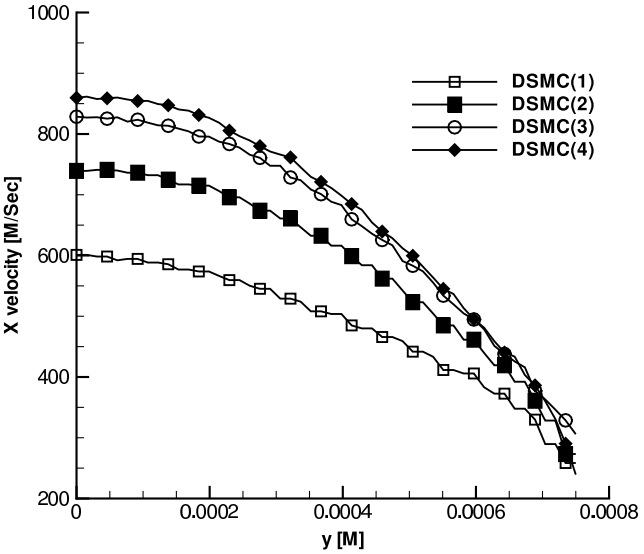

Fig. 12 DSMC, X-velocity profiles across the nozzle exit. The nozzle axis is located at $y = 0$.

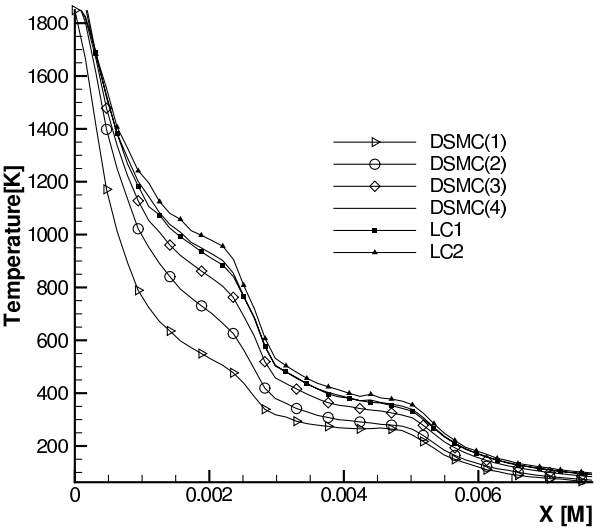

Fig. 13 DSMC, translational temperature along the nozzle centerline. The nozzle throat and exit are located at ∼0.0027 and ∼.005 m, respectively.

parameters given in Table 2 for each of the four DSMC calculations using the relationships that

$$\Delta V \propto \frac{1}{N_{\text{cells}}} \tag{6}$$

$$\frac{1}{N} \propto F_{\text{num}} \tag{7}$$

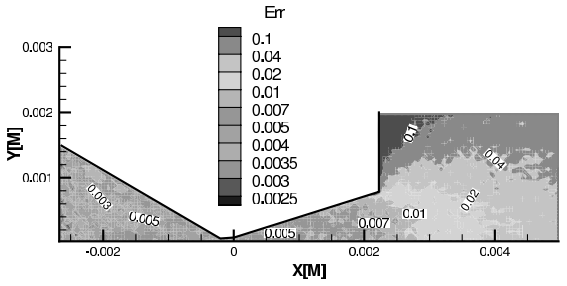

Fig. 14 DSMC(1), relative statistical error in temperature, $Err(T_{M_s})$.

where N_{cells} and F_{num} are the number of collisional cells at steady state and the ratio of physical to computational particles, respectively.

The most rigorous application of Eq. (5) would require one to evaluate ΔV and N for each collisional cell in the computational domain, that is, at the local cell conditions. However, in practice there is no guarantee that each of the four DSMC cases would have the identical computational mesh of collision cells at steady state, due to automatic grid adaptation. Therefore, the average, overall numerical parameters, such as those given in Table 2, are used in Eq. (6) instead of the local collision cell values. That this approach is reasonable may be understood in terms of the mesh adaptation technique used in the SMILE DSMC software tool [18] which keeps the number of particles per collisional cell approximately the same for all of the collision cells in the computational domain. (Division of "number of particles" by "number of cells" values given in the columns of Table 2 shows that for the four simulation cases the average number is about two particles per collision cell.) For each successive case in Table 2, greater grid adaptation is allowed thereby generating more collision cells and more computational particles. Because the computational domain remains the same for all four cases, the collisional cell size is inversely proportional to the number of collisional cells. Similarly, the total number of particles in the computational domain N, among the four cases is inversely proportional to F_{num} because the number of true particles is a constant for all four cases because it is determined by the single stagnation condition considered in this work.

Figure 13 also shows the two derived temperature profiles A_0, designated linear combination 1 (LC1) and LC2, obtained by using Eq. (5) to take linear combinations of the DSMC(1)–DSMC(4) results. As discussed previously, average computational parameter values are used leading to a single 3×3 matrix of ΔV and N values for the entire computational grid to obtain A_0 for each linear combination. The first linear combination LC1 was based on the results of the cases DSMC(1)–DSMC(3) and the second one, LC2, was based on the cases DSMC(2)–DSMC(4). For each linear combination, there are three unknowns A_0, A_2, and A_3 so that three DSMC solutions are required. Figure 13 shows that the LC1 and LC2 temperature profiles are found to be close to those of the best of the DSMC cases, DSMC(4). In the region of most importance (from the nozzle throat to the exit) LC1 and LC2 are found to be in agreement within 5%. Although LC2 is a bit higher than DSMC(4), it still agrees with it also within 5%. In comparison, the level of agreement between the best two successive DSMC calculations, DSMC(3) and (4) in the same spatial region, is only about 10%. The improved level of agreement between the two linear combination cases suggests that the linear dependence model for the deterministic errors due to particle and spatial discretization may reasonably be represented by

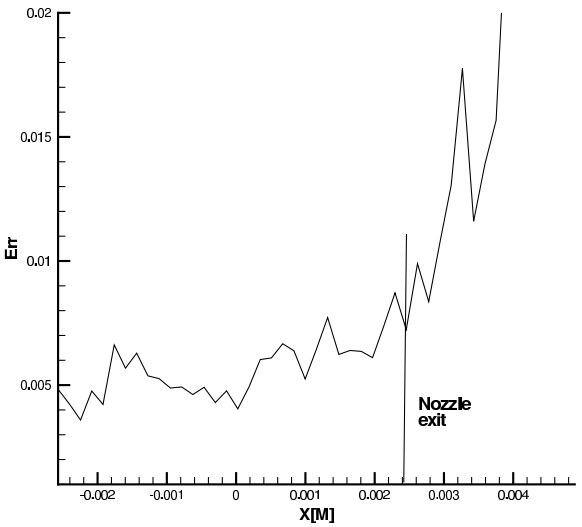

Fig. 15 DSMC(1) relative statistical error, $Err(T_{M_s})$, along the nozzle centerline.

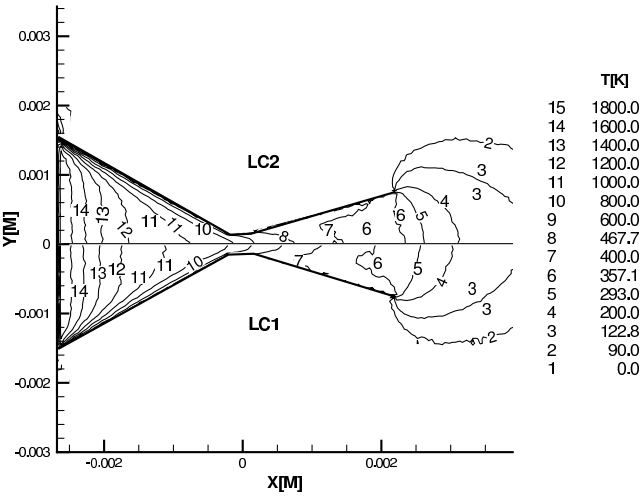

Fig. 16 DSMC(1), LC1, and LC2, translational temperature fields.

Eq. (5). Figure 16 presents a comparison of the temperature fields between these two linear combination cases, LC1 and LC2. The good agreement between the two fields also provides confidence that the DSMC(4) solution is converged to about 10%.

V. Conclusions

The careful study of a low stagnation pressure micronozzle case showed that when 1.3×10^8 simulation particles, distributed over 5.23×10^7 cells, are used in the baseline DSMC method, strict flowfield convergence cannot be obtained. Even though the major DSMC requirements of time step and number of particles in a computational cell are satisfied in all the calculations, quantitative changes of the flow parameters are evident by improvement of the numerical parameters from the low-resolution mesh case DSMC(1) to a higher-resolution mesh case DSMC(4). The thrust at the nozzle exit is an important system performance metric. Table 2 shows the thrust computed for the low- and high-resolution DSMC cases. Consistent with Figs. 11 and 12, the boundary layer is reduced as the number of particles increases. The flow viscosity is modeled better from the DSMC(1) to the DSMC(4) case and the thrust increases by 17%. However, thrust is a spatially averaged quantity dependent upon pressure and velocities and is therefore less sensitive to numerical errors, as may be seen in the variation for the four cases shown in Table 2.

Characterization of the numerical errors suggests that the solution is accurate because the statistical errors in temperature are quite small and the deterministic ones are in a linear regime. The statistical errors for the temperature fields were estimated effectively and were found to be relatively small compared to the deterministic errors. The fact that the deterministic errors depend linearly on the numerical parameters allows us to understand how close to the final convergent solution we are. In the presented case the final result is close to being converged because the difference between the two linear combinations and the results obtained from the most expensive DSMC calculation are close. Although our main goal here was to investigate the flow in a MEMS micronozzle device, this developed technique for assessing numerical errors is general and can be used to check the results of the DSMC method for other computationally intensive problems.

Acknowledgement

This research performed at the Pennsylvania State University was supported by the U.S. Air Force Office of Scientific Research Grant No. F49620-02-1-0104 administered by Mitat Birkan.

References

[1] Reed, B., De Groot, W., and Dang, L., "Experimental Evaluation of Cold Flow Micronozzles," AIAA Paper 2001-3521, July 2001.

[2] Mueller, J., Chakraborty, I., Bame, D., and Tang, W., "Vaporizing Liquid Microthruster Concept—Preliminary Results of Initial Feasibility Studies," *Micropropulsion for Small Spacecraft*, edited by M. Micci, and A. Ketsdever, Vol. 187, Progress in Astronautics and Aeronautics, AIAA, Reston, VA, 2000, pp. 215–230.
[3] Alexeenko, A., Collins, R., Gimelshein, S., Levin, D., and Reed, B., "Numerical Modeling of Axisymmetric and Three-Dimensional Flows in MEMS Nozzles," *AIAA Journal*, Vol. 40, No. 5, 2002, pp. 897–904.
[4] Alexeenko, A., Levin, D., Fedosov, D., Gimelshein, S., and Collins, R., "Coupled Thermal-Fluid Modeling of Micronozzles for Performance Analysis in MEMS-Based Thruster," AIAA Paper 2003-4717, 2003.
[5] Alexeenko, A., Fedosov, D., Levin, D., Gimelshein, S., and Collins, R., "Performance Analysis of Microthrusters Based on Coupled Thermal-Fluid Modeling and Simulation," *Journal of Propulsion and Power*, Vol. 21, No. 1, 2005, pp. 95–101.
[6] Ketsdever, A., Glabough, M., Gimelshein, S., and Alexeenko, A. A.,"Experimental and Numerical Determination of Micropropulsion Device Efficiencies at Low Reynolds Numbers," *AIAA Journal*, Vol. 43, No. 3, March 2005, pp. 633–641.
[7] Bayt, R., and Breuer, K., "Viscous Effects in Supersonic MEMS-Fabricated Micronozzles," *Proceedings of the 3rd Microfluids Symposium*, American Society of Mechanical Engineers, New York, Nov. 1998.
[8] Chen, K., Winter, M., and Huang, R., "Supersonic Flow in Miniature Nozzles of the Planar Configuration," *Journal of Micromechanics and Microengineering*, Vol. 15, March 2005, pp. 1736–1744.
[9] Bird, G., *Molecular Gas Dynamics and the Direct Simulation of Gas Flows*, Clarendon, Oxford, England, U.K., 1994.
[10] Fedosov, D., *Investigation of Numerical Errors in Direct Simulation Monte Carlo Method*, Ph.D. Thesis, Pennsylvania State University, University Park, PA, 2004.
[11] Fedosov, D., Rogasinsky, S., Zeifman, M., Ivanov, M., Alexeenko, A., and Levin, D., "Analysis of Numerical Errors in the DSMC Method," *Proceedings of the 24th International Symposium on Rarefied Gas Dynamics*, American Institute of Physics, New York, May 2005.
[12] Shreider, Y., *Method of Statistical Testing, Monte Carlo Method*, Elsevier, Amsterdam, 1964.
[13] Parzen, E., *Method of Statistical Testing, Monte Carlo Method, Modern Probability Theory and Its Applications*, Wiley, New York, 1960.
[14] Ermakov, S., and Mikhailov, G., *Statistical Modeling*, Nauka, Moscow, 1982 (in Russian).
[15] Ivanov, M., and Rogasinsky, S. V.,"Analysis of Numerical Techniques of the Direct Simulation Monte Carlo Method in the Rarefied Gas Dynamics," *Soviet Journal of Numerical Analysis and Mathematical Modeling*, Vol. 3, No. 6, 1988, pp. 453–465.
[16] Wilcox, D., *Basic Fluid Mechanics*, 2nd ed., DCW Industries, Inc., La Canada, CA, 2000.
[17] Roache, P., *Computational Fluid Dynamics*, Hermosa Publishers, Albuquerque, NM, 1972.
[18] Ivanov, M., and Gimelshein, S., "Current Status and Prospects of the DSMC Modeling of Near-Continuum Flows of Non-Reacting and Reacting Gases," *Proceedings of the Rarefied Gas Dynamics 23rd International Symposium, AIP Conference*, Vol. 663, AIP, New York, 2003, pp. 339–348.
[19] Ivanov, M., and Rogasinsky, S., "Analysis of Numerical Techniques of the Direct Simulation Monte Carlo Method in the Rarefied Gas Dynamics," *Soviet Journal of Numerical Analysis and Mathematical Modeling*, Vol. 3, No. 6, 1988, pp. 453–456.